Functional Models for Catechol 1,2-Dioxygenase. Structure, Reactivity, and Mechanism

Lawrence Que, Jr.,* Richard C. Kolanczyk, and Lloyd S. White

Contribution from the Department of Chemistry, University of Minnesota, Minneapolis, Minnesota 55455-2120. *Received December 17, 1986*

Abstract: A series of $[Fe(L)DBC]^{2-}$ complexes, where L is a tetradentate tripodal ligand and DBC is 3,5-di-*tert*-butylcatecholate, has been synthesized and characterized by visible spectroscopy and cyclic voltammetry. The tripodal ligands are derivatives of NTA, nitrilotriacetic acid, where one of the carboxymethyl arms has been replaced by a 2-hydroxybenzyl group. Crystals of $(dabcoH)_2[Fe(NTA)DBC]$ ($P2_1/n$; dabco, 1,4-diazabicyclo[2.2.2]octane) reveal a six-coordinate high-spin ferric complex with an unsymmetrically chelated DBC ($r_{Fe-O(DBC)}$ = 1.889, 1.979 Å). The visible spectra of the complexes exhibit catecholate-to-Fe(III) charge-transfer transitions in the 600-nm region, while their cyclic voltammograms show a reversible wave near 0 V vs. SCE due to the semiquinone/catecholate couple. The energy of the LMCT band and the $E^{\circ\prime}$ value for a particular complex shift in response to the Lewis acidity of the metal center, as expected. These complexes react with dioxygen over a period of days to yield two identified products, 3,5-di-*tert*-butylmuconic anhydride (trapped as the furanone) and 3,5-di-*tert*-butyl-2-hydroxy-*p*-benzoquinone. The product yields depend on the Lewis acidity of the metal center, with the NTA complex yielding the highest amount of anhydride (ca. 80%) and essentially no quinone. As the Lewis acidity of the metal center diminishes, the amount of anhydride decreases and the yield of quinone increases. These observations are interpreted in light of the substrate activation mechanism proposed for the catechol dioxygenases; important features include the reaction of a monodentate catecholate–iron(III) complex with O_2 to form an iron peroxide intermediate and its subsequent metal-facilitated decomposition to the anhydride.

The oxidative cleavage of catechols by non-heme iron dioxygenases is part of nature's mechanism for metabolizing aromatic compounds.[1] The enzymes, catechol 1,2-dioxygenase and protocatechuate 3,4-dioxygenase, catalyze the intradiol cleavage of catechols to *cis,cis*-muconic acids via a mechanism involving a high-spin ferric center.[2] A variety of studies indicate the active-site iron remains in the ferric oxidation state throughout the course of mechanism.[3-10] Mössbauer spectra of the native enzymes, enzyme–substrate complexes, and two oxygenated intermediates generated under steady-state conditions all exhibit magnetic hyperfine splitting at liquid-helium temperatures, indicative of high-spin ferric iron.[3-5] Raman studies show the coordination of tyrosine and substrate catechol to the metal center in the ES complex.[6,7] The presence of these ligands lowers the Fe(III)/Fe(II) redox potential and renders the iron(III) center difficult to reduce under biological conditions.[8] The coordination of tyrosine also gives rise to phenolate-to-iron(III) ligand-to-metal charge-transfer transitions (LMCT), which persist throughout the reaction cycle, even in the short-lived intermediates observed with stopped-flow-kinetic methods.[9,10] We have thus proposed a scheme, consistent with the observations, involving substrate activation rather than oxygen activation.[11] In this scheme, the substrate catecholate loses both its protons upon coordination to the iron and becomes susceptible to reaction with oxygen to yield a peroxide intermediate. This intermediate then decomposes to product.

The mechanism we have proposed would seem to be prone to a biomimetic approach since no other cofactors are required for the enzyme reaction, and this has been the focus of our recent efforts. Other workers in this field have developed catechol cleavage systems utilizing copper,[12] ruthenium,[13] vanadium[14] and iron[15-18] complexes. Two of the iron systems are particularly interesting. Funabiki and co-workers have reported a catalytic mixture consisting of $FeCl_3$, bipyridine, and pyridine which converts 3,5-di-*tert*-butylcatechol into intradiol cleavage products.[15] Other products isolated from the reaction mixture indicate that this system is also capable of extradiol cleavage[2] mimicking such enzymes as catechol 2,3-dioxygenase and protocatechuate 4,5-dioxygenase. Weller and Weser[18] found that Fe(NTA)[19] can catalyze intradiol cleavage as well. We have isolated the cate-

(1) Dagley, S. In *The Bacteria*; Ornsten, L. N.; Sokatch, J. R., Eds.; Academic: New York, 1978; Vol. 6, pp 305–368.
(2) For a recent review of these enzymes, see Que, L., Jr. *Adv. Inorg. Biochem.* **1983**, *5*, 167–199.
(3) Que, L., Jr.; Lipscomb, J. D.; Zimmermann, R.; Münck, E.; Orme-Johnson, W. H.; Orme-Johnson, N. R. *Biochim. Biophys. Acta* **1976**, *452*, 320–334.
(4) Whittaker, J. W.; Lipscomb, J. D.; Kent, T. A.; Münck, E. *J. Biol. Chem.* **1984**, *259*, 4466–4475.
(5) Kent, T. A.; Münck, E.; Pyrz, J. W.; Widom, J.; Que, L., Jr. *Inorg. Chem.* **1987**, *26*, 1402–1408.
(6) Felton, R. H.; Cheung, L. D.; Phillips, R. S.; May, S. W. *Biochem. Biophys. Res. Commun.* **1978**, *85*, 844–850.
(7) Que, L., Jr.; Heistand, R. H., II *J. Am. Chem. Soc.* **1979**, *101*, 2219–2221.
(8) Pyrz, J. W.; Roe, A. L.; Stern, L. J.; Que, L., Jr. *J. Am. Chem. Soc.* **1985**, *107*, 614–620.
(9) Bull, C.; Ballou, D. P.; Otsuka, S. *J. Biol. Chem.* **1981**, *256*, 12681–12686.
(10) Walsh, T. A.; Ballou, D. P.; Mayer, R.; Que, L., Jr. *J. Biol. Chem.* **1983**, *258*, 14422–14427.
(11) Que, L., Jr.; Lipscomb, J. D.; Münck, E.; Wood, J. M. *Biochim. Biophys. Acta* **1977**, *485*, 60–74.
(12) (a) Tsuji, J.; Takayanagi, H. *J. Am. Chem. Soc.* **1974**, *96*, 7349–7350. (b) Tsuji, J.; Takayanagi, H.; Sakai, I. *Tetrahedron Lett.* **1975**, 1245–1246. (c) Rogic, M. M.; Demmin, T. R. *J. Am. Chem. Soc.* **1978**, *100*, 5472–5487. (d) Demmin, T. R.; Swerdloff, M. D.; Rogic, M. M. *J. Am. Chem. Soc.* **1981**, *103*, 5795–5804. Brown, D. G.; Beckmann, L.; Ashby, C. H.; Vogel, G. C.; Reinprecht, J. T. *Tetrahedron Lett.* **1977**, 1363–1364.
(13) Matsumoto, M.; Kuroda, K. *J. Am. Chem. Soc.* **1982**, *104*, 1433–1434.
(14) Tatsuno, Y.; Tatsuda, M.; Otsuka, S. *J. Chem. Soc., Chem. Commun.* **1982**, 1100–1101. Tatsuno, Y.; Tatsuda, M.; Otsuka, S.; Tani, K. *Inorg. Chim. Acta* **1983**, *79*, 104–105.
(15) Funabiki, T.; Mizoguchi, A.; Sugimoto, T.; Tada, S.; Tsuji, M.; Sakamoto, H.; Yoshida, S. *J. Am. Chem. Soc.* **1986**, *108*, 2921–2932. Funabiki, T.; Mizoguchi, A.; Sugimoto, T.; Yoshida, S. *Chem. Lett.* **1983**, 917–920. Funabiki, T.; Sakamoto, H.; Yoshida, S.; Tarama, K. *J. Chem. Soc., Chem. Commun.* **1979**, 754–755.
(16) Nishida, Y.; Shimo, H.; Kida, S. *J. Chem. Soc., Chem. Commun.* **1984**, 1611–11612.
(17) Russo, U.; Vidali, M.; Zarli, B.; Purrello, R.; Maccarrone, G. *Inorg. Chim. Acta* **1986**, *120*, L11–L13.
(18) Weller, M. G.; Weser, U. *J. Am. Chem. Soc.* **1982**, *104*, 3752–3754. Weller, M. G.; Wesser, U. *Inorg. Chim. Acta* **1985**, *107*, 243–245.
(19) Abbreviations used: NTA, *N,N*-bis(carboxymethyl)glycine; HDA, *N*-(*o*-hydroxybenzyl)-*N*-(carboxymethyl)glycine; Bu_2HDA, *N*-(4,6-di-*tert*-butyl-2-hydroxybenzyl)-*N*-(carboxymethyl)glycine; Cl_2HDA, *N*-(4,6-dichloro-2-hydroxybenzyl)-*N*-(carboxymethyl)glycine; salen, *N,N'*-ethylenebis(salicylideneamine); $DBCH_2$, 3,5-di-*tert*-butylcatechol; $catH_2$, catechol; DBSQ, 3,5-di-*tert*-butyl-*o*-benzosemiquinone; DBQ, 3,5-di-*tert*-butyl-*o*-benzoquinone; pip, piperidine; pyrr, pyrrolidine, dabco, 1,4-diazabicyclo-[2.2.2]octane; TBAF, tetrabutylammonium tetrafluoroborate; SCE, saturated calomel electrode; EDTA, *N,N'*-ethylenebis(*N*-(carboxymethyl)glycine); HEDTA, *N,N'*-ethylene-*N*-(carboxymethyl)glycine-*N'*-(hydroxyethyl)glycine; bpy, 2,2'-bipyridine; ehpg, *N,N'*-ethylenebis[2-(*o*-hydroxyphenyl)glycine]; HXTA, *N,N'*-(2-hydroxy-5-methyl-1,3-xylylene)bis(*N*-(carboxymethyl)-glycine); Me_3tacn, 1,4,7-trimethyl-1,4,7-triazacyclononane; TCE, 1,1,2,2-tetrachloroethane; Hacac, 2,4-pentanedione; py, pyridine; phen, 1,10-phenanthroline; salpr, aminobis(*N*-3-propylsalicylideneamine).

0002-7863/87/1509-5373$01.50/0

cholate complex of Fe(NTA) and characterized it structurally;[20] this complex reacts with dioxygen to afford the desired intradiol cleavage product. We have extended our study to catecholate complexes of other tetradentate ligands; the variation in cleavage yield and side products obtained indicates that the iron coordination environment plays an important role in determining the outcome of this reaction. Our observations allow us to further refine the proposed substrate activation mechanism for the enzymes.[11]

Experimental Section

Ligands. HDA was synthesized according to the method of Martell.[21] $NaBu_2HDA$ was synthesized by the addition of 0.05 mol of 2,4-di-*tert*-butylphenol and 0.05 mol of iminodiacetic acid to a solution of 0.125 mol of NaOH in 60 mL of H_2O/95% EtOH (1:2). The reaction mixture was warmed to 50 °C, and 7 mL of 37% formaldehyde solution (0.08 mol) was added. After being heated for 6 h, the reaction mixture was cooled overnight to yield a white solid, which was washed with 95% EtOH. ^1H NMR in D_2O: δ 1.23 (s, 9 H), 1.37 (s, 9 H), 3.22 (s, 4 H), 3.82 (s, 2 H), 7.06–7.33 (m, 2 H). $NaCl_2HDA$ was synthesized similarly by using 2,4-dichlorophenol as starting material. ^1H NMR in D_2O: δ 3.60 (s, 4 H), 4.21 (s, 2 H), 7.09–7.40 (m, 2 H).

Complexes. Fe(salen)DBCH[22] was synthesized according to published procedures, and [Fe(salen)DBC]$^-$ was generated by treating Fe(salen)-DBCH with piperidine in DMF under N_2, yielding a green solution. The complex exhibited absorption maxima at 343, 386, and 637 nm, similar to that of K[Fe(salen)DBC].[22]

Q_2[Fe(NTA)DBC] was synthesized by heating $Fe(NTA)(H_2O)_2$, $DBCH_2$, and the appropriate secondary amine (piperidine, pyrrolidine, or dabco) in a 1:1:2 molar ratio in DMF under N_2 for an hour. After filtering, the solution was cooled slowly to yield crystals of the desired compound. X-ray quality crystals were obtained from the dabcoH$^+$ salt. It is important to use $Fe(NTA)(H_2O)_2$ as starting material in order to obtain products of good crystallinity. $Fe(NTA)(H_2O)_2$ was obtained by reacting $Fe(ClO_4)_3 \cdot 6H_2O$ and Na_3NTA in water. The desired complex precipitated after 20 min; this was washed with water and dried. Anal. Calcd for $Fe(NTA)(H_2O)_2$ ($C_6H_{10}FeNO_8$): C, 25.74; H, 3.60; N, 5.00. Found: C, 26.01; H, 3.81; N, 5.16. Anal. Calcd for $(dabcoH)_2$[Fe(NTA)DBC]·DMF ($C_{35}H_{53}FeN_6O_9$): C, 55.48; H, 7.05; N, 11.09. Found: C, 55.16; H, 7.10; N, 11.25. Anal. Calcd for $(pipH)_2$[Fe(NTA)DBC]·DMF ($C_{33}H_{57}FeN_4O_9$): C, 55.85; H, 8.10; N, 7.89. Found: C, 56.11; H, 7.95; N, 7.86. Anal. Calcd for $(pyrrH)_2$[Fe(NTA)DBC]·DMF ($C_{31}H_{53}FeN_4O_9$): C, 54.63; H, 7.84; N, 8.22. Found: C, 54.89; H, 7.60; N, 8.22.

$(pyrrH)_2$[Fe(L)DBC], where L = Bu_2HDA and Cl_2HDA, were synthesized in a manner similar to that for $(pyrrH)_2$[Fe(NTA)DBC] starting with $FeL(H_2O)_2$. The aquo complexes precipitated out of aqueous solutions of $Fe(ClO_4)_3 \cdot 6H_2O$ and the tetradentate ligand. $(pyrrH)_2$[Fe(HDA)DBC] was obtained by reacting equimolar quantities of $HDAH_2$, $DBCH_2$, and $Fe(ClO_4)_3 \cdot 6H_2O$ with a sixfold excess of pyrrolidine in DMF under N_2. The reaction mixture was maintained at 70 °C for $2^1/_2$ h and then filtered. Upon cooling, a green microcrystalline solid was obtained. The crystals were washed with DMF and then dried in vacuo. Anal. Calcd for [$Fe(Bu_2HDA)(CH_3OH)_2$] ($C_{21}H_{34}FeNO_7$): C, 53.86; H, 7.32; N, 2.99. Found: C, 53.59; H, 7.11; N, 3.04. Anal. Calcd for [$Fe(Cl_2HDA)(H_2O)_2$] ($C_{11}H_{12}Cl_2FeNO_7$): C, 33.28; H, 3.05; N, 3.53. Found: C, 33.46; H, 3.00; N, 3.59. Anal. Calcd for $(pyrrH)_2$[Fe(HDA)DBC] ($C_{33}H_{50}FeN_3O_7$): C, 60.36; H, 7.67; N, 6.40. Found: C, 60.43; H, 7.48; N, 6.69. Anal. Calcd for $(pyrrH)_2$[Fe(Bu_2HDA)DBC]·DMF ($C_{44}H_{73}FeN_4O_8$): C, 62.77; H, 8.74; N, 6.65. Found: C, 63.15; H, 8.65; N, 6.67. Anal. Calcd for $(pyrrH)_2$[Fe(Cl_2HDA)DBC] ($C_{33}H_{48}Cl_2FeN_3O_7$): C, 54.63; H, 6.67; N, 5.79. Found: C, 54.63; H, 6.69; N, 5.90.

X-ray diffraction data were collected on an Enraf-Nonius CAD4 X-ray diffractometer using Mo Kα (λ = 0.71069 Å) radiation out to 2θ = 48°. The structure was solved by Patterson and Fourier methods and refined anisotropically to a final value of R_1 of 0.067. The final difference map did not reveal any chemically significant electron density; the most intense peak was found in the vicinity of the disordered DMF solvate with an intensity of 0.436 e/Å^3.

UV–visible spectra were obtained on an HP 8451 diode array spectrophotometer. NMR spectra were obtained on an IBM WM-200 or WM-300 spectrometer. IR spectra were obtained on a Perkin-Elmer 1710 FT-IR spectrometer, while mass spectra were run at the University of Minnesota Mass Spectroscopy Facility using Finnigan 4000 and AEI MS-30 spectrometers. Electrochemical measurements were obtained in DMF solution with 0.1 M TBAF on a BAS100 electrochemical analyzer using a Pt working electrode and an SCE reference electrode. The ferricinium/ferrocene couple was measured under the same conditions to enable future corrections for junction potentials (+0.498 V).[23a]

The reactions with O_2 were run under ambient conditions in an atmosphere of pure oxygen. The reactions were acidified to pH 3 with HCl when the characteristic green color of the catecholate complexes had faded (ca. 4 days). The organic products were extracted from the DMF/water solution with ether (3 × 100 mL), dried over anhydrous $MgSO_4$, and then concentrated. The product mixture was subjected to reverse phase isocratic HPLC separation (Waters 6000A isocratic system; Kratos 769Z variable wavelength detector, 240 nm; Whatman Partisil ODS-5 C18 column) with a solvent mixture consisting of $CH_3CN/CH_3OH/H_2O/CH_3COOH$ (33:33:33:1). The products eluted were compared with known standards where possible. Unanticipated products were isolated by preparative HPLC and identified by using their UV–visible, IR, NMR, and mass spectra. Spectral data for 3,5-di-*tert*-butyl-2-hydroxy-*p*-benzoquinone: UV–vis λ_{max} (cyclohexane) 264, 394 nm;[23b] ^1H NMR ($CDCl_3$) 1.28 (s, 9 H), 1.36 (s, 9 H), 6.50 (s, 1 H), 7.18 (s, 1 H, D_2O exchangeable); CI-MS *m/e* 237 (M + 1), 221 (M − CH_3), 181 (M + 1 − C_4H_8).

Scheme I

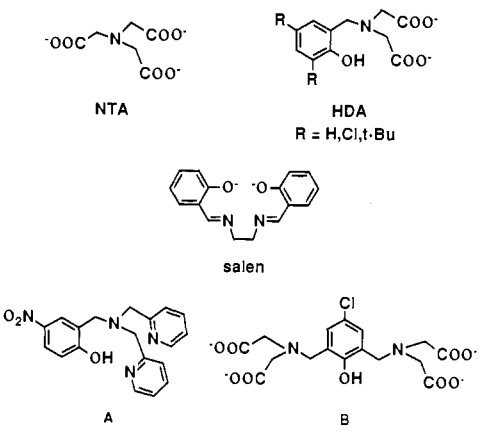

Results and Discussion

Synthesis and Characterization. A series of catecholate complexes with various tetradentate ligands has been synthesized and structurally characterized to serve as functional models for the catechol dioxygenases. Among the five ligands investigated are the linear tetradentate salen ligand and four tripodal ligands, NTA, HDA, Cl_2HDA, and Bu_2HDA (Scheme I). Only DBC complexes have been studied because the *tert*-butyl groups minimize possible side reactions and facilitate product identification. [Fe(salen)-DBC]$^-$ has been previously characterized[22] and is presumed to have a chelated catecholate ligand by analogy to the crystallographically determined [Fe(salen)cat]$^-$.[24] This coordination mode is characterized by absorption maxima near 380 and 650 nm, associated with the salen and catecholate LMCT bands, respectively.[8] In previous studies, [Fe(salen)DBC]$^-$ was obtained by the addition of KO-*t*-Bu to Fe(salen)DBCH, while the complex has been generated by the addition of excess piperidine in the current study. Some variation in the catecholate λ_{max} is observed as a function of counterion due to the association of the cation with the anionic complex; in the crystal structure of K[Fe(salen)cat], a K atom is clearly coordinated to a trigonal face derived from salen and catechol oxygens.[24]

The catecholate complexes with tetradentate tripodal ligands are synthesized by the addition of 3,5-di-*tert*-butylcatechol and

(20) White, L. S.; Nilsson, P. V.; Pignolet, L. H.; Que, L., Jr. *J. Am. Chem. Soc.* **1984**, *106*, 8312–8313.
(21) Harris, W. R.; Motekaitis, J. J.; Martell, A. E. *Inorg. Chem.* **1975**, *14*, 974–978.
(22) Heistand, R. H., II; Lauffer, R. B.; Fikrig, E.; Que, L., Jr. *J. Am. Chem. Soc.* **1982**, *104*, 2789–2796.
(23) (a) Gagne, R. R.; Koval, C. A.; Lisensky, G. C. *Inorg. Chem.* **1980**, *19*, 2854–2855. (b) Musso, H.; Zunker, R. *Liebigs Ann. Chem.* **1968**, *717*, 64–72.
(24) Lauffer, R. B.; Heistand, R. H., II; Que, L., Jr. *Inorg. Chem.* **1983**, *22*, 50–55.

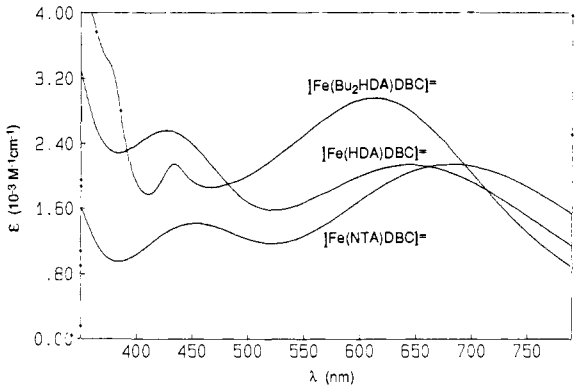

Figure 1. Visible spectra of $[Fe(L)DBC]^{2-}$ complexes in MeOH.

Table I. Spectral and Electrochemical Data for the $[Fe(L)DBC^{2-}$ Complexes

complex	λ_{max}, nm (MeOH)	λ_{max} nm (DMF)	$E^{\circ\prime}$ (mV (DMF)[a]
$[Fe(NTA)DBC]^{2-}$	682	625	+59
$[Fe(Cl_2HDA)DBC]^{2-}$	666	622	-33
$[Fe(HDA)DBC]^{2-}$	643	580	-111
$[Fe(Bu_2HDA)DBC]^{2-}$	613	566	-136
$[Fe(salen)DBC]^{-}$	...	637	-98

[a] The $E^{\circ\prime}$ for the Fc^+/Fc couple under these conditions is +498 mV. The tripodal ligand complexes exhibited peak separations of 70 ± 3 mV, while the salen complex exhibited a peak separation of 100 mV.

a secondary amine in DMF under anaerobic conditions to a solution or suspension of FeL in DMF. The components all dissolve upon mixing and warming to form a dark green solution, from which crystals of the desired complex are harvested. A full description of the structure of $(dabcoH)_2[Fe(NTA)DBC]$ is presented in the next section. The complex is six-coordinate, and the corresponding HDA derivatives are assumed to have similar structures.

The visible spectra of the tripodal ligand complexes are characterized by two absorption features (Figure 1 and Table I). $[Fe(NTA)DBC]^{2-}$ exhibits bands at 458 and 688 nm; since NTA is not expected to be chromophoric in the visible region, the visible features are assigned to DBC-to-iron(III) LMCT transitions, by analogy to the $[Fe(cat)_3]^{3-}$ spectrum.[25] For the HDA complexes, the HDA ligand gives rise to an LMCT band that overlaps with the higher energy LMCT band. In all these complexes, the energy of the lower energy LMCT band shows a dependence on the nature of the tetradentate ligand. For the HDA series, the band shifts to higher energy as the ring substituents become more electron donating. This trend is in line with the decreasing Lewis acidity of the iron center, which would raise the energy of the metal d orbitals. The NTA complex, having the least Lewis basic tetradentate ligand, gives rise to the lowest energy LMCT band. A similar correlation has been found for phenolate LMCT bands in Fe(salen)X complexes.[8]

Electrochemical information on these complexes provides further insight (Table I). The cyclic voltammogram for $[Fe(Cl_2HDA)DBC]^{2-}$, shown in Figure 2, features a quasi-reversible redox process near −35 mV vs. SCE and an irreversible oxidation near +700 mV, which generates a reduction near −300 mV on the return scan. The reversible process is associated with the coordinated DBSQ/DBC couple. Scanning to more positive potential oxidizes the bound DBSQ to DBQ, and the complex decomposes. The free DBQ is then reduced on the return scan to DBSQ. Redox chemistry at the iron center is obscured by the presence of ammonium ions. The other complexes exhibit similar values for the coordinated DBSQ/DBC couple, which are significantly shifted to more positive potentials than that observed for the reduction of free $DBSQ^-$ to DBC^{2-}.[26] The large positive

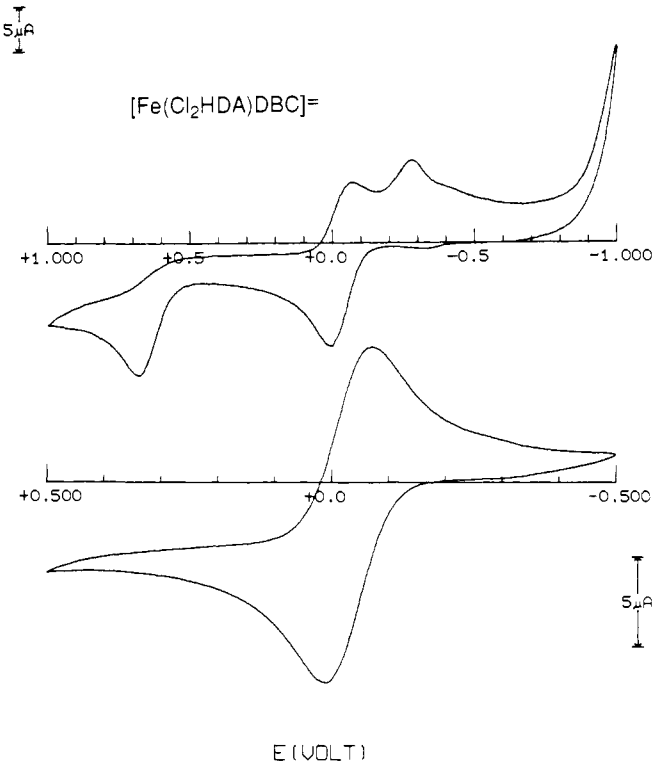

Figure 2. Cyclic voltammetry of $[Fe(Cl_2HDA)DBC]^{2-}$ in DMF with 0.1 M TBAF as supporting electrolyte. Potentials are referenced vs. SCE with no correction for junction potential. $E^{\circ\prime}$ for the ferricinium/ferrocene couple under these conditions is +498 mV.

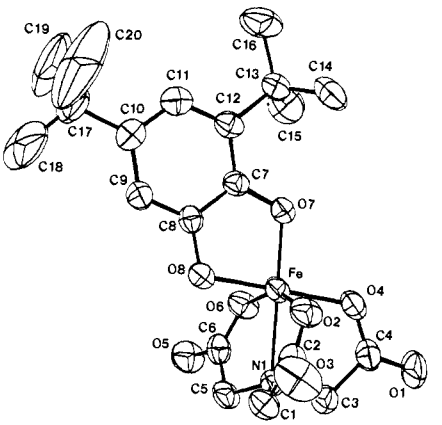

Figure 3. Structure of $[Fe(NTA)DBC]^{2-}$ showing 50% probability thermal ellipsoids and atom labeling scheme. Hydrogen atoms have been omitted for clarity.

shift indicates that the chelation of the catecholate to the iron significantly stabilizes the DBC oxidation level and reflects the strong affinity of catecholates for iron(III).[27] The potentials observed also reflect the Lewis acidity of metal center as modulated by the tetradentate ligand. Complexes of the less basic ligands exhibit more positive DBSQ/DBC potentials, indicating a greater stabilization of the DBC oxidation state by the more Lewis acidic iron center. The trend in potentials follows the trend in the DBC π LMCT band energies and also mirrors similar correlations made for iron(III) phenolate complexes.[8]

Crystal Structure of $(dabcoH)_2[Fe(NTA)DBC]\cdot DMF$. Crystals of $(dabcoH)_2[Fe(NTA)DBC]\cdot DMF$ were obtained from DMF solution as six-sided plates in the space group $P2_1/n$. The structure

(25) Salama, S.; Stong, J. D.; Neilands, J. B.; Spiro, T. G. *Biochemistry* **1978**, *17*, 3781–3785.

(26) Nanni, E. J., Jr.; Stallings, M. D.; Sawyer, D. T. *J. Am. Chem. Soc.* **1980**, *102*, 4481–4485.

(27) Avdeef, A.; Sofen, S. R.; Bregante, T. L.; Raymond, K. N. *J. Am. Chem. Soc.* **1978**, *100*, 5362–5370. Lloret, F.; Mollar, M.; Moratal, J.; Faus, J. *Inorg. Chim. Acta* **1986**, *124*, 67–74.

Table II. Crystallographic Data for $(dabcoH)_2[Fe(NTA)DBC]\cdot DMF$

formula	$C_{35}H_{53}FeN_6O_9$
M_r	763.74
space group	$P2_1/n$
a, Å	17.874 (4)
b, Å	9.963 (3)
c, Å	23.117 (9)
α, deg	90.0
β, deg	105.4 (1)
γ, deg	90.0
V, Å^3	3969
Z	4
D_{calc}, g/cm^3	1.278
radiation used	Mo Kα (λ = 0.71073 Å)
max [(sin θ)λ]	0.57
cryst size, mm^3	0.30 × 0.45 × 0.16
μ, cm^{-1}	4.328
no. of reflctns measd	6225
reflctns used[a]	3413 [$(F_o)^2 \geq 1\sigma(F_o)^2$]
no. of variables used	415
R[b]	0.067
R_w[b]	0.073
GOF[b]	1.733
p[a]	0.05

[a] The intensity data were processed as described in: *CAD 4 and SDP-PLUS User's Manual*; B. A. Frenz & Assoc.; College Station, TX, 1982. The net intensity $I = [K(NPI)](C - 2B)$, where K = 20.1166 (attenuator factor), NPI = ratio of fastest possible scan rate to scan rate for the measurement, C = total count, and B = total background count. The standard deviation in the net intensity is given by $[\sigma(I)]^2 = (k/NPI)^2[C + 4B + (pI)^2]$, where p is a factor used to downweight increase reflections. The observed structure factor amplitude F_o is given by $F_o = (I/Lp)^{1/2}$, where Lp = Lorentz and polarization factors. The $\sigma(I)$'s were converted to the estimated errors in the relative structure factors $\sigma(F_o)$ by $\sigma(F_o) = {}^1/_2[\sigma(I)/I]F_o$. [b] The function minimized was $\sum w(|F_o| - |F_c|)^2$, where $w = 1/[\sigma(F_o)]^2$. The unweighted and weighted residuals are defined as $R = (||F_o| - |F_c||)/\sum|F_o|$ and $R_w = [(\sum w(|F_o| - |F_c|))^2/(\sum w|F_o|)^2]^{1/2}$. The error is an observation of unit weight (GOF) is $[\sum w(|F_o| - |F_c|)^2/(NO - NV)]^{1/2}$, where NO and NV are the number of observations and variables, respectively.

of the anion is shown in Figure 3, together with the numbering scheme for the molecule. Crystallographic data can be found in Table II. Atomic coordinates and selected bond distances and bond angles are given in Tables III and IV, respectively, while the list of the thermal parameters can be found in Table S-1 (supplementary material).

The complex is best described as a distorted octahedron, with C_s symmetry in the optimum conformation. The plane is defined by the catecholate ring, Fe, N1, and O4. The catecholate is chelated, and the NTA acts as a tetradentate tripodal ligand. The N–Fe–O(NTA) angles range from 77° to 82.5°, and the iron is 0.45Å above the plane defined by the three coordinated NTA oxygens. This is a result of the constraints imposed by the tripodal tetradentate coordination of the NTA and also observed for other complexes of tripodal ligands such as $[Fe(EDTA)H_2O]^-$[28] and $[(FeHEDTA)_2O]^{2-}$.[29]

The bond distances observed for this complex are mostly unremarkable. The C–O bond lengths for the coordinated DBC (1.349 (5) and 1.338 (5) Å) are as expected for chelated catecholates (1.361 Å for $[Mn(DBC)_3]^{2-}$,[30] 1.338 and 1.364 Å for [Cu(bpy)DBC],[31] 1.349 Å for $[Cr(cat)_3]^{3-}$,[32] 1.338 Å for $[Fe(cat)_3]^{3-}$[32]). All other DBC bond lengths are normal. The iron–carboxylate bonds in $[Fe(NTA)DBC]^-$ range in length from 2.002 to 2.039 Å compared with 2.042 Å for $Mg[Fe((R,R)\text{-ehpg})]_2$,[33] 1.97 Å for $[Fe_2(HXTA)(OH)(H_2O)_2]$,[34] and 2.11 Å for $[Fe_4(HXTA)_2O_2(OH)_2]^{4-}$.[34] The Fe–N bond at 2.224 (3) Å in $[Fe(NTA)DBC]^-$ is as expected for an Fe–N(tertiary amine) bond (2.198 and 2.268 Å for $[(FeMe_3tacn)_2O(OAc)_2]^{2+}$[35]), though shorter than that in a comparable tripodal ligand (2.32 Å for $[Fe(EDTA)H_2O]^-$[28]).

The most interesting structural feature of $[Fe(NTA)DBC]^{2-}$ is the difference in the Fe–O(DBC) bond lengths. The Fe–O trans to the N (1.887 Å) is nearly 0.1 Å shorter than that trans to the carboxylate (1.979 Å), a difference significantly larger than the esd's. Previous studies of mononuclear catecholate complexes have not uncovered such a large difference. The longer Fe–O(DBC) bond in $[Fe(NTA)DBC]^{2-}$ resembles those found for other iron catecholate complexes, e.g., 2.015 Å for $[Fe(cat)_3]^{3-}$,[32] 1.988 Å for $[Fe(salen)cat]^-$,[24] 1.95 and 1.97 Å for $[Fe_2(cat)_4OAc]^{3-}$.[36] The large difference in the Fe–O(DBC) bond lengths in $[Fe(NTA)DBC]^{2-}$ does not appear to be due to steric constraints. If this were a determining factor, the Fe–O7 bond, which is adjacent to the 3-*tert*-butyl group, would be expected to be the longer bond. Indeed, it is the shorter bond. The strong Fe–O(DBC) bond may be a result of the weak Fe–N interaction trans to the Fe–O bond.

The accuracy of this structure (R = 6.7, R_w = 7.3) is limited by some disorder present in the 5-*tert*-butyl positions of the DBC ligand, the cations, and the solvent of crystallization. The DMF molecule could be fit with six non-hydrogen atoms, two of which had assigned occupancy factors of 0.5.

Prior to this study, crystals of $(pyrrH)_2[Fe(NTA)DBC]$ were obtained as thin, square plates, assigned to the space group $P2_1$. The structure of the anion was found to be similar to that of the dabco salt but could not be refined below R = 14% at room temperature. Attempts to collect data at low temperature were unsuccessful.

Reactivity Studies. We have investigated the reactivity of catecholate complexes with O_2 in DMF, and they all react. The nature of the products and their respective yields depend on the nature of the tetradentate ligand (Table V). The cleavage products observed are all derivatives of 3,5-di-*tert*-butyl-5-(carboxymethyl)-2-furanone; depending on the nucleophiles present, the parent acid and various amides can be identified in the product mixtures. This product mixture indicates that the immediate product of oxidative cleavage is the muconic anhydride; the furanones are then derived from nucleophilic attack on the less hindered carbonyl of the anhydride, followed by cyclization, i.e., eq 1. Some $DBCH_2$ is observed in the product mixtures; since

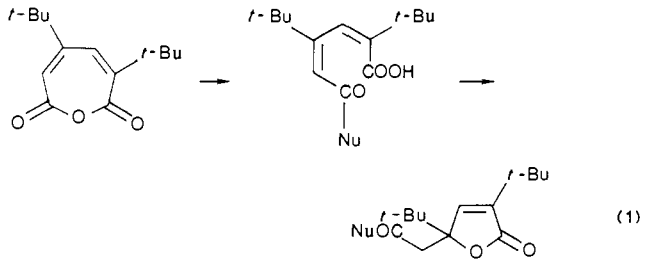

(1)

there is no corresponding amount of DBQ, DBSQ appears to be an unlikely intermediate and the $DBCH_2$ presumably arises from unreacted complex. 3,5-Di-*tert*-butyl-2-hydroxy-*p*-benzoquinone, identified by its UV–visible, NMR, and mass spectra, is observed in the reaction of the HDA complexes. The remainder of the carbon balance cannot be observed in the HPLC traces and is ascribed to polymeric products of the reactions.

(28) Lind, M. D.; Hoard, J. L.; Hamor, M. J., Hamor, T. A. *Inorg. Chem.* **1964**, *3*, 34–43.
(29) Lippard, S. J.; Schugar, H.; Walling, C. *Inorg. Chem.* **1967**, *6*, 1825–1831.
(30) Hartman, J. R.; Foxman, B. M.; Cooper, S. R. *Inorg. Chem.* **1984**, *23*, 1381–1387.
(31) Buchanan, R. M.; Wilson-Blumenberg, C.; Trapp, C.; Larsen, S. K.; Greene, D. L.; Pierpont, C. G. *Inorg. Chem.* **1986**, *25*, 3070–3076.
(32) Raymond, K. N.; Isied, S. S.; Brown, L. D.; Fronczek, F. R.; Nibert, J. H. *J. Am. Chem. Soc.* **1976**, *98*, 1767–1774.
(33) Bailey, N. A.; Cummins, D.; McKenzie, E. D.; Worthington, J. M. *Inorg. Chim. Acta* **1981**, *50*, 111–120.
(34) Murch, B. P.; Boyle, P. D.; Que, L., Jr. *J. Am. Chem. Soc.* **1985**, *107*, 6728–6729.
(35) Chaudhuri, P. D.; Weighardt, K.; Nuber, B.; Weiss, J. *Angew. Chem., Int. Ed. Engl.* **1985**, *24*, 778–779.
(36) Anderson, B. F.; Webb, J.; Buckingham, D. A.; Robertson, G. B. *J. Inorg. Biochem.* **1982**, *16*, 21–32.

Table III. Atomic Complexes for $(dabcoH)_2[Fe(NTA)DBC]\cdot DMF$

atom	*x*	*y*	*z*	*B*, Å^2	atom	*x*	*y*	*z*	*B*, Å^2
Fe	0.07406 (5)	0.21230 (9)	0.12396 (3)	3.34 (2)	H1	0.1718	0.0906	0.0063	8*
N1	0.1027 (2)	0.2146 (4)	0.0360 (2)	2.88 (9)	H1′	0.0940	0.0243	0.0082	8*
C1	0.1348 (3)	0.0818 (6)	0.0289 (2)	3.8 (1)	H3	0.1362	0.3945	0.0167	8*
C2	0.1745 (3)	0.0201 (6)	0.0904 (3)	4.1 (1)	H3′	0.2025	0.2894	0.0293	8*
O1	0.2484 (3)	0.4544 (5)	0.1129 (2)	6.9 (1)	H5	0.0038	0.1667	−0.0246	8*
O2	0.1608 (2)	0.0746 (4)	0.1357 (2)	4.2 (1)	H5′	0.0412	0.2972	−0.0407	8*
C3	0.1601 (3)	0.3233 (6)	0.0423 (2)	4.0 (1)	H9	−0.1054	−0.1096	0.1163	8*
C4	0.1925 (3)	0.3815 (6)	0.1048 (3)	4.1 (1)	H11	−0.1113	0.0020	0.2826	8*
O3	0.2146 (3)	−0.0803 (4)	0.0915 (2)	6.9 (1)	H14	0.0993	0.2453	0.3664	8*
O4	0.1564 (2)	0.3539 (4)	0.1439 (2)	4.2 (1)	H14′	0.0946	0.0978	0.3443	8*
C5	0.0296 (3)	0.2477 (6)	−0.0092 (2)	3.9 (1)	H14″	0.1078	0.2128	0.3028	8*
C6	−0.0234 (3)	0.3302 (6)	0.0177 (2)	3.6 (1)	H15	−0.0077	0.4068	0.3212	8*
O5	−0.0829 (2)	0.3774 (4)	−0.0166 (2)	5.2 (1)	H15′	−0.0006	0.3735	0.2574	8*
O6	−0.0068 (2)	0.3406 (4)	0.0743 (2)	4.10 (9)	H15″	−0.0799	0.3581	0.2722	8*
O7	0.0501 (2)	0.2152 (4)	0.1987 (1)	3.87 (9)	H16	−0.0234	0.2290	0.3897	8*
O8	−0.0021 (2)	0.0639 (4)	0.1049 (2)	3.95 (9)	H16′	−0.0975	0.1811	0.3425	8*
C7	−0.0050 (3)	0.1253 (5)	0.2022 (2)	3.1 (1)	H16″	−0.0315	0.0800	0.3696	8*
C8	−0.0331 (3)	0.0427 (5)	0.1508 (2)	3.0 (1)	H18	−0.2433	−0.3156	0.1508	8*
C9	−0.0876 (3)	−0.0544 (6)	0.1507 (2)	3.5 (1)	H18′	−0.2309	−0.1876	0.1162	8*
C10	−0.1176 (3)	−0.0734 (6)	0.2002 (3)	3.9 (1)	H18″	−0.1649	−0.2928	0.1353	8*
C11	−0.0904 (3)	0.0117 (6)	0.2492 (2)	4.1 (1)	H19	−0.2816	−0.1927	0.2199	8*
C12	−0.0338 (3)	0.1107 (6)	0.2519 (2)	3.5 (1)	H19′	−0.2285	−0.0836	0.2577	8*
C13	−0.0050 (3)	0.2024 (7)	0.3069 (2)	4.5 (1)	H19″	−0.2693	−0.0572	0.1907	8*
C14	0.0823 (4)	0.1883 (8)	0.3325 (3)	6.7 (2)	H20	−0.1803	−0.3497	0.2495	8*
C15	−0.0253 (4)	0.3495 (7)	0.2876 (3)	6.7 (2)	H20′	−0.0991	−0.3231	0.2394	8*
C16	−0.0430 (4)	0.1702 (8)	0.3570 (3)	7.3 (2)	H20″	−0.1268	−0.2402	0.2867	8*
C17	−0.1773 (4)	−0.1813 (6)	0.2021 (3)	5.6 (2)	H21A	0.3714	0.4559	0.2745	8*
C18	−0.2070 (6)	−0.249 (1)	0.1463 (5)	20.1 (3)	H21A′	0.2978	0.4020	0.2286	8*
C19	−0.2457 (4)	−0.123 (1)	0.2189 (5)	14.8 (3)	H22A	0.3725	0.2976	0.1851	8*
C20	−0.1427 (7)	−0.283 (1)	0.2495 (7)	20.0 (5)	H22A′	0.4450	0.3354	0.2361	8*
N2A	0.3259 (3)	0.2938 (5)	0.3053 (2)	3.9 (1)	H23A	0.2310	0.2029	0.2502	8*
C21A	0.3445 (4)	0.3773 (6)	0.2573 (3)	4.6 (2)	H23A′	0.2691	0.1160	0.3059	8*
C22A	0.3949 (4)	0.2960 (7)	0.2273 (3)	6.0 (2)	H24A	0.3320	0.0092	0.2528	8*
C23A	0.2789 (3)	0.1738 (6)	0.2761 (3)	4.8 (2)	H24A′	0.3897	0.1958	0.3779	8*
C24A	0.3262 (4)	0.1000 (7)	0.2400 (3)	5.8 (2)	H25A′	0.4318	0.3209	0.3619	8*
C25A	0.4002 (4)	0.2460 (7)	0.3461 (3)	5.3 (2)	H26A	0.4931	0.1903	0.3163	8*
C26A	0.4417 (4)	0.1576 (7)	0.3109 (3)	6.3 (2)	H26A′	0.4435	0.0685	0.3256	8*
N3A	0.4025 (3)	0.1577 (5)	0.2472 (2)	4.6 (1)	H21B	0.6213	0.3671	0.0061	8*
N2B	0.6879 (3)	0.2764 (6)	0.0781 (3)	7.6 (2)	H21B′	0.6313	0.2149	−0.0036	8*
C21B	0.6573 (5)	0.295 (1)	0.0128 (4)	11.7 (3)	H22B	0.7235	0.2546	−0.0448	8*
C22B	0.7198 (5)	0.326 (1)	−0.0183 (4)	9.2 (3)	H22B′	0.7081	0.4070	−0.0403	8*
C23B	0.7441 (5)	0.176 (1)	0.0869 (5)	11.6 (3)	H23B	0.7195	0.0945	0.0709	8*
C24B	0.8079 (5)	0.2079 (9)	0.0575 (4)	9.3 (3)	H23B′	0.7658	0.1659	0.1290	8*
C25B	0.7199 (5)	0.400 (1)	0.0951 (4)	12.6 (3)	H24B	0.8565	0.2073	0.0870	8*
C26B	0.7827 (5)	0.440 (1)	0.0678 (4)	13.0 (3)	H24B′	0.8083	0.1420	0.0279	8*
N3B	0.7950 (3)	0.3396 (5)	0.0296 (2)	6.0 (1)	H25B	0.7406	0.3992	0.1374	8*
					H25B′	0.6797	0.4649	0.0844	8*
					H26B	0.7679	0.5206	0.0456	8*
					H26B′	0.8288	0.4548	0.0986	8*
					CY1	0.4302 (5)	0.196 (1)	0.0576 (4)	8.9 (3)*
					CY2	0.4979 (9)	0.192 (2)	0.1124 (7)	18.0 (5)*
					CY3	0.382 (1)	0.106 (2)	0.0639 (8)	23.5 (7)*
					CY4	0.340 (1)	0.292 (2)	−0.002 (1)	12.2 (7)*
					CY5	0.418 (1)	0.316 (2)	0.028 (1)	28 (1)*
					CY6	0.322 (2)	0.138 (3)	0.005 (1)	16 (1)*

[a] Atoms with an asterisk were refined isotropically anisotropically refined atoms are given in the form of the isotropic equivalent thermal parameter defined as $(^4/_3)$ $[a^2B(1,1) + b^2B(2,2) + c^2B(3,3) + ab(\cos\gamma)B(1,2) + ac(\cos\beta)B(1,3) + bc(\cos\alpha)B(2,3)]$.

$[Fe(NTA)DBC]^{2-}$ reacts with O_2 over a period of 4 days, by which time the characteristic green color of the catecholate complex has faded. This complex yields the largest amount of cleavage product at ca. 80%. ^{18}O-labeling studies of the $[Fe(NTA)DBC]^{2-}$ reaction show the incorporation of a single label into the product; the label is localized in the carboxylate oxygens of the furanone on the basis of the mass spectral fragmentation pattern.[20] This supports the proposition that the muconic anhydride is the product of this reaction. Table VI compares this labeling result with our results on other catechol cleavage systems. Of those studied, the NTA reaction is by far the only one that yields such a clean label incorporation; the others all show some label scrambling. The implications of these observations will be discussed in the next section.

The HDA complexes also react with O_2 over a period of 4 days, but the yields of cleavage products are smaller than that for NTA. Furthermore, the cleavage yields decrease as the HDA phenolate becomes more electron donating, and the yield of the *p*-quinone increases. Indeed, the quinone is the major identifiable product of the Bu_2HDA reaction.

$[Fe(salen)DBC]^-$ reacts with O_2 to produce a yield of cleavage product that is intermediate between those of the HDA and the Cl_2HDA complexes. We earlier reported the lack of reactivity of this complex toward O_2; those experiments were done in THF over a period of hours, during which no spectral changes were observed. However, over a period of 6 days, a small amount of cleavage product could be detected in THF; the yield increases to ca. 30% in DMF. There is no evidence in the salen reaction for the *p*-quinone byproduct found in the HDA reactions, but we do observe a new HPLC peak with a retention time close to that of the *p*-quinone; the nature of this product and its mechanism of formation has yet to be determined.

The results of our work on the O_2 reactivity of isolated DBC complexes can be compared to those of catalytic systems consisting

Table IV. Selected Bond Distances and Bond Angles for $(dabcoH)_2[Fe(NTA)DBC]\cdot DMF$

	Bond Lengths (Å)		
Fe-N1	2.224 (3)	O2-C2	1.261 (6)
Fe-O2	2.034 (3)	C2-O3	1.227 (5)
Fe-O4	2.002 (3)	C2-C1	1.537 (6)
Fe-O6	2.039 (3)	C1-N1	1.469 (5)
Fe-O7	1.887 (3)	O4-C4	1.270 (5)
Fe-O8	1.979 (3)	C4-O1	1.210 (5)
C7-O7	1.349 (5)	C4-C3	1.521 (6)
C8-O8	1.338 (5)	C3-N1	1.473 (5)
C7-C8	1.424 (6)	O6-C6	1.266 (5)
C8-C9	1.372 (6)	C6-O5	1.238 (5)
C9-C10	1.399 (6)	C6-C5	1.507 (6)
C10-C11	1.395 (6)	C5-N1	1.478 (5)
C11-C12	1.402 (6)		
C12-C7	1.385 (6)		
	Bond Angles (deg)		
N1-Fe-O2	77.1 (1)	Fe-O7-C7	113.1 (3)
N1-Fe-O4	82.5 (1)	Fe-O8-C8	110.3 (3)
N1-Fe-O6	77.3 (1)	Fe-N1-C1	106.5 (3)
N1-Fe-O7	178.5 (1)	Fe-N1-C3	103.9 (2)
N1-Fe-O8	96.6 (1)	Fe-N1-C5	105.9 (3)
O2-Fe-O4	87.6 (1)	Fe-O2-C2	119.3 (3)
O4-Fe-O6	93.2 (1)	Fe-O4-C4	118.0 (3)
O6-Fe-O8	90.0 (1)	Fe-O6-C6	117.9 (3)
O8-Fe-O2	88.9 (1)	O7-C7-C8	115.8 (4)
O7-Fe-O8	84.6 (1)	O8-C8-C7	116.3 (4)

Table V. Summary of Product Yields (%) for the $[Fe(L)DBC]^{2-}$ Complexes[a]

complex	$E^{\circ\prime}$, mV	furanone	quinone	$DBCH_2$
$[Fe(NTA)DBC]^{2-}$	+59	84	<1	1
$[Fe(Cl_2HDA)DBC]^{2-}$	-33	57	6	6
$[Fe(HDA)DBC]^{2-}$	-111	33	4	5
$[Fe(Bu_2HDA)DBC]^{2-}$	-136	12	19	4
$[Fe(salen)DBC]^{-}$ (DMF)	-98	35	<1	7
$[Fe(salen)DBC]^{-}$ (THF)		22	<1	3

[a] All reactions were run under 1 atm of O_2 for 4–6 days, during which time the characteristic DBC LMCT color had faded. Furanone refers to (3,5-di-*tert*-butyl-2-furanon-5-yl)acetic acid amides, and quinone refers to 3,5-di-*tert*-butyl-2-hydroxyl-*p*-benzoquinone. Some $DBCH_2$ was recovered and is presumably derived from unreacted complex, since no DBQ was observed in the reaction mixture.

of Fe(III) coordinated to one or more ligands and $DBCH_2$. To date there have been four reported involving the following ligands: NTA,[18] ligand A,[16] ligand B,[17] and a bpy/py mixture[15] (Scheme I).

The reaction time and the yield of furanone from the $[Fe(NTA)DBC]^{2-}$ reaction are comparable to those reported by Weller and Weser[18] in their experiments involving catalytic amounts of Fe(NTA) in a borate buffer/(DMF or MeOH) solvent mixture. (The borate buffer was designed to prevent oxidation of $DBCH_2$ to DBQ in the reaction medium.) The similarity of the results suggests that $[Fe(NTA)DBC]^{2-}$ is the active species in the catalytic mixture.

The introduction of a phenolate to the iron coordination environment diminishes the yield of cleavage product in both the stoichiometric and catalytic systems, with the catalytic systems being much less effective at cleaving the catechol with yields of 10–16% and a substantial amount of DBQ (40–85%) observed.[16,17] Perhaps the most complex of the catalytic systems is that devised by Funabiki and co-workers[15] where an array of products is observed, including species proposed to arise from extradiol cleavage of the catechol. The presumed coordination environment of the iron in this system differs substantially from that in our complexes. This difference serves to further emphasize the role the iron ligands play in determining the course of the reaction.

Mechanistic Considerations. The pattern of reactivity observed for the five DBC complexes investigated provides us with insight into the mechanism of oxidative cleavage by Fe(III) complexes. The identity and yields of the products show a systematic dependence on the nature of the tetradentate ligand, indicating that the coordination chemistry of the iron(III) center plays a role in determining the course of the O_2 reaction. The chelated DBC complexes are all six-coordinate high-spin iron(III) complexes and all exhibit catecholate-to-Fe(III) charge transfer transitions which reflect the relative Lewis acidities of the ferric centers. There is no apparent tendency for the ferric center to be reduced; indeed catecholate coordination is expected to stablize the ferric state.[28,37] The enzyme-substrate complexes of catechol 1,2-dioxygenase and protocatechuate 3,4-dioxygenase have been similarly characterized as high spin ferric complexes.[3-5] These observations serve to support the proposed substrate activation mechanism[11] (Scheme II). In this mechanism, the substrate catechol coordinates to the metal center in a monodentate fashion, losing both its OH protons. The iron–catechol complex then reacts with O_2 to yield an intermediate peroxide complex, which then decomposes to form the muconic anhydride. The anhydride is then cleaved by oxide (or hydroxide) bound to the metal center, giving rise to product.

Scheme II

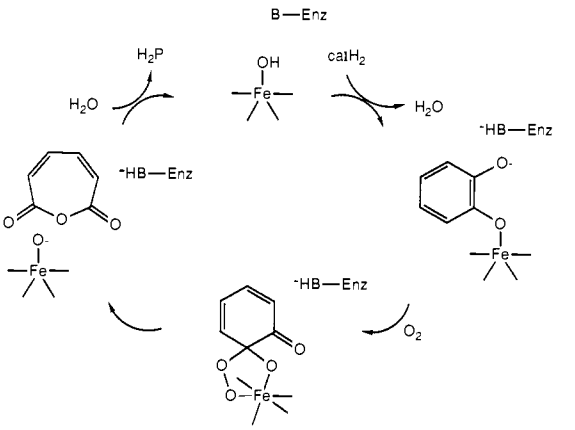

The novel aspect of this mechanism is the role ascribed to the iron(III) center, and our observations support this proposed role. The fact that these high-spin ferric complexes react at all shows that the chemistry proposed for the enzyme active site can occur in a model system, albeit much less efficiently. A key intermediate in this mechanism is the peroxide complex; its participation is mechanistically required for the oxygenation reaction. Similar species have been proposed in the oxygenations of phenols and indoles;[38-41] in the case of the oxygenation of 2,4,6-tri-*tert*-butylphenol by Co(salpr), the metal peroxide complex has been crystallized.[41] In our $[Fe(L)DBC]^{2-}$ studies, we propose that the increased yield of desired cleavage product with increased Lewis acidity of the metal center reflects the coordination of the intermediate peroxide to the metal center. The interaction of the Lewis basic peroxide with a metal center having enhanced Lewis acidity and oxophilicity during the reaction would serve to promote its formation.

The formation of the peroxide complex requires the reduction of dioxygen. The electrochemical results on the DBC complexes suggest that outer-sphere electron transfer from the chelated DBC complex to O_2 is unlikely, since the DBSQ/DBC couples of the complexes are less reducing than the O_2/O_2^- couple[42] in protic and aprotic solvents. In support of this, we have demonstrated that superoxide reduces Fe(salen)DBSQ to $[Fe(salen)DBC]^-$ in THF solution.[43] So a structural change would seem necessary

(37) Cooper, S. R.; McArdle, J. V.; Raymond, K. N. *Proc. Natl. Acad. Sci. U.S.A.* **1978**, *75*, 3551–3554.
(38) Muto, S.; Bruice, T. C. *J. Am. Chem. Soc.* **1982**, *104*, 2284–2290.
(39) Muto, S.; Bruice, T. C. *J. Am. Chem. Soc.* **1980**, *102*, 7559–7564.
(40) Nishinaga, A.; Itahara, T.; Shimizu, T.; Matsuura, T. *J. Am. Chem. Soc.* **1978**, *100*, 1821–1825.
(41) Nishinaga, A.; Tomita, H.; Nishizawa, K.; Matsuura, T.; Ooi, S.; Hirotsu, K. *J. Chem. Soc., Dalton Trans.* **1981**, 1504–1514.
(42) Fee, J. A.; Valentine, J. S. In *Superoxide and Superoxide Dismutases*; Michelson, A. M., McCord, J. M., Fridovich, I., Eds.; Academic: New York, 1977; pp 19–60.

Table VI. Summary of ^{18}O-Labeling Experiments for DBC Cleavage Systems

system	product[a]	mass distributn of molecular ion				mass distributn of m/z 195 fragment[b]		
		M + 1	M + 3	M + 5	M + 7	195	197	199
$[Fe(NTA)DBC]^{2-}$/DMF	a	2	98	...	...	2	98	...
$RuCl_2(PPh_3)_3$/TCE[13]	b	18	70	11	...			
		12	76	12	...			
$VO(acac)_2/CH_2Cl_2$[14]	b	8	88	3	...			
		7	90	3	...			
		10	86	4	...			
$FeCl_2$/bpy/py/THF[15]	c	3	88	9	...	3	89	8
		3	89	8	...	3	89	7
Cu(phen)DBC/Me_2SO[12e]	c	68	27	5	...	75	20	5
		84	15	1	...	85	14	1
$Co(C_5H_5)_2$/THF[44]	c	22	48	26	4	36	50	13
		24	45	26	5	40	49	11

[a] Products designated a, b, and c are (3,5-di-*tert*-butyl-2-furanon-5-yl)acetic acid piperidinamide, 3,5-di-*tert*-butylmuconic anhydride, and (3,5-di-*tert*-butyl-2-furanon-5-yl)acetic acid, respectively. [b] The m/z 195 fragment corresponds to the 3,5-di-*tert*-butyl-2-furanonyl ion.

to make the complex more reducing.

The formation of the peroxide complex from the chelated catecholate complex and dioxygen would require an available coordination site on the iron center; this site could be made available by the dissociation of one DBC oxygen from the metal center at some point of the reaction. The monodentate DBC^{2-} would no longer be stabilized by chelation and thus be a better reductant. This proposed dissociation was suggested by the crystal structure of $[Fe(NTA)DBC]^{2-}$, which shows an unsymmetrically chelated DBC, since this complex was the first crystallographically characterized Fe(III) complex to show cleavage activity.[20] In $[Fe(NTA)DBC]^{2-}$, the Fe–O7 bond is longer than the Fe–O8 bond by 0.09 Å; thus, the Fe–O7 bond would break prior to the reaction with O_2.

The HDA complexes presumably have unsymmetrically chelated DBC ligands as well because the HDA ligands are simply variations of the NTA ligand. However, the unsymmetrically chelated DBC appears not to be a requirement for reactivity, since $[Fe(salen)DBC]^-$ also reacts with O_2 under the same conditions. By analogy to the crystal structure of $[Fe(salen)cat]^-$,[25] the DBC ligand is probably symmetrically chelated in $[Fe(salen)DBC]^-$. The solubility of $[Fe(salen)DBC]^-$ in THF and DMF affords a further test of the proposed mechanism. The greater reactivity of the complex in DMF is consistent with the bond-breaking initial step, since the more polar solvent would be expected to stabilize the monodentate DBC configuration.

We propose that the monodentate DBC complex is the O_2-reactive species. We conceive this reaction as the addition of O_2 to the iron catecholate complex, forming the C–O and the Fe–O bonds simultaneously or in close succession. In the process, two electrons from the catecholate are transferred to O_2 resulting in a peroxide complex. The singlet–triplet forbiddenness of the O_2 reaction is relaxed because the substrate gains some radical character by the delocalization of unpaired spin density onto the substrate via the catecholate LMCT interaction. The NMR contact shifts observed for the catecholate protons in the synthetic complexes provide ample proof of this.[22] Initial O_2 attack on the catecholate would be analogous to the reaction of dihydroflavin[38] or semiquinone[44] with O_2, both of which are rapid. The resulting peroxide would then be coordinated by the metal center and thus stabilized. Alternatively, O_2 attack at the metal center is conceivable because the charge-transfer interaction would introduce some ferrous character to the metal center. This would result in the formation of a semiquinone–Fe(III)–superoxide species, which could then collapse to the peroxide–Fe(III) species via radical coupling. We cannot distinguish between the two alternatives, but we favor the attack of O_2 on the substrate.

2,6-Di-*tert*-butyl-3-hydroxy-*p*-benzoquinone is a product observed only in the reactions of the HDA complexes. It presumably

Scheme III

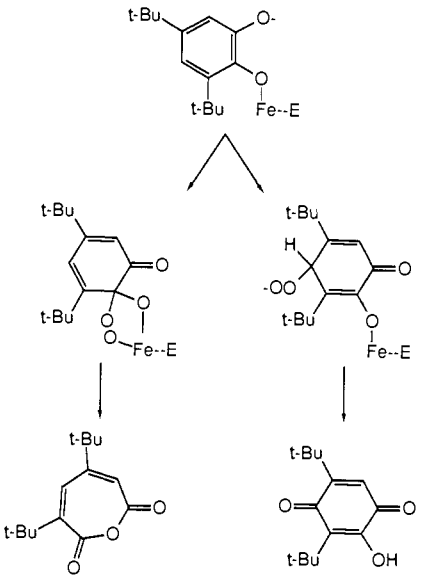

results from O_2 attack at C-4 of DBC, instead of C-1 or C-2 and subsequent decomposition of the C-4 peroxide, i.e., eq 2.

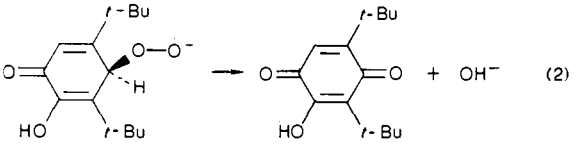

(2)

The possibility of different sites of O_2 attack has been previously demonstrated by Nishinaga et al. in the oxygenations of 2,4,6-trisubstituted phenols, which can occur at C-2 or C-4 depending on the reaction conditions.[40] A mechanism that would explain the formation of both the furanone and quinone products requires the formation of the monodentate DBC, with O-2 coordinated to the metal center (Scheme III). Ketonization of O-1 would result in electron density being concentrated on C-2 or the vinylogous C-4. O_2 attack at C-2 would result in the formation of the furanones, while attack at C-4 would result in the quinone. The monodentate DBC complex proposed is precisely that which would result from the breaking of the longer Fe–O(DBC) bond in $[Fe(NTA)DBC]^{2-}$ (Fe–O7).

However, the quinone is observed only in the HDA reactions and the yield is greatest with the Bu_2HDA complex. Its absence in the NTA reaction and the trend of increasing yield in the HDA reactions as the ring substituents become more electron donating indicate that the Lewis acidity of the metal center plays a role in determining the products of the reaction. The more Lewis acidic Fe(NTA) center promotes the attack of O_2 at C-2 by coordinating

(43) Lauffer, R. B.; Heistand, R. H.; Que, L., Jr. *J. Am. Chem. Soc.* **1981**, *103*, 3947–3949.
(44) White, L. S.; Que, L., Jr. *J. Mol. Catal.* **1985**, *33*, 139–149.

the intermediate peroxide; this would explain the high yield of furanone product for the NTA complex. O_2 attack at C-4 becomes a more viable alternative as the Lewis acidity of the metal center, and consequently its oxophilicity, diminishes.

The tetradentate salen ligand represents a different coordination environment from that of the tripodal ligand. Its DBC LMCT band and its DBSQ/DBC potential indicate that the iron center has a Lewis acidity comparable to that of the HDA complex. The yield of furanone from the salen complex is comparable to that of the HDA complex. However, no *p*-quinone is observed in the salen reaction indicating a difference in mechanism. Since [Fe(salen)DBC]$^-$ probably has a structure where the two Fe–O-(DBC) bonds are of equal length, perhaps formation of the less sterically hindered O-1 coordinated DBC configuration is favored; such a species could not give rise to O_2 attack at C-4. The appearance of yet a different product is interesting; its identity and the mechanism for its formation are under investigation.

In the proposed mechanism for intradiol cleavage of DBC to the furanone, the Lewis acidity of the metal center also plays a role in facilitating the decomposition of the peroxide intermediate to the muconic anhydride. The labeling studies summarized in Table VI support this role for the iron center. Except for the Fe(NTA) reaction, all others studied show evidence for label scrambling. A significant amount of unlabeled product is observed in these reactions, as is overlabeled product. For example, some of the muconic anhydride derived from the Ru and V reactions are doubly labeled, where only one label would be expected. Some of the furanone from the $FeCl_2$/bpy/py reaction is doubly labeled. At first glance, this is not an unexpected result for a dioxygenase mimic; one ^{18}O label would be expected in the furanone ring and the other on the carboxymethyl side chain. But closer scrutiny of the fragmentation pattern in the mass spectrum shows that both labels are incorporated into the furanone ring, indicating that some of the precursor anhydride is doubly labeled, as in the Ru and V cases.

We have shown that label scrambling occurs when the peroxy intermediate is free in solution.[44] This is particularly true for the $Co(C_5H_5)_2$ system where the meatl center is clearly coordinatively saturated and incapable of coordinating another ligand. In only the Fe(NTA) system is this label scrambling not observed. We believe that this is due to the metal center binding the peroxide strongly and facilitating its decomposition by providing a site that stabilizes the incipient oxide which forms in the peroxide rearrangement.

By incorporating the foregoing observations with recent spectroscopic data on the enzymes, our original proposed mechanism can be refined in the following manner. The ferric center in the catechol 1,2-dioxygenase active site would serve two functions. First, the metal center would serve to coordinate and activate the substrate by promoting the loss of both catecholate protons and delocalizing unpaired spin density into the catechol ring. Substrate coordination to the active site metal is confirmed by the observation of resonance enhanced Raman vibrations from the substrate resulting from the irradiation of the catecholate-to-Fe(III) charge-transfer band.[7] Spin delocalization into the substrate is indicated by the paramagnetically shifted NMR resonances of the bound catecholate in the enzyme–substrate complex;[45] they also indicate that the catecholate is coordinated in a monodentate fashion. This complex would then react with O_2 to form a peroxy intermediate. The metal center then serves to promote the decomposition of the peroxide to yield the anhydride intermediate and then the expected product. Thus two aspects of the ferric center are important—its Lewis acidity and the accesibility of LMCT states. In future studies, the relative importance of these two properties will be clarified by investigating the reactivity of corresponding Ga(III) complexes.

Acknowledgment. This work has been supported by the National Institutes of Health (GM-33162). L.Q. is grateful for an Alfred P. Sloan Research Fellowship (1982–1986) and an NIH Research Career Development Award (1982–1987). We thank Professors L. H. Pignolet and J. D. Britton and Mr. P. V. Nilsson for their efforts on the crystallographic studies and Professor L. L. Miller for the use of the BAS100 analyzer.

Registry No. $Fe(NTA)(H_2O)_2$, 67359-33-5; $Fe(Bu_2HDA)(H_2O)_2$, 109282-11-3; $Fe(Cl_2HDA)(H_2O)_2$, 109282-12-4; $(dabcoH)_2$[Fe(NTA)-DBC]·DMF, 93862-86-3; $(pipH)_2$[Fe(NTA)DBC], 81770-38-9; $(pyrrH)_2$[Fe(NTA)DBC], 109282-06-6; $(pyrrH)_2$[Fe(Bu_2HDA)DBC], 109282-08-8; $(pyrrH)_2$[Fe(Cl_2HDA)DBC], 109282-10-2; $(pyrrH)_2$[Fe-(HDA)DBC], 109282-14-6; Fe(salen)DBCH, 109282-15-7; [Fe(salen)-DBC]$^-$, 78165-60-3; O_2, 7782-44-7; 3,5-di-*tert*-butyl-2-hydroxy-*p*-benzoquinone, 21243-82-3; *N*-[2-(3,5-di-*tert*-butyl-2-furanon-5-yl)-acetyl]pyrrolidine, 109244-01-1; catechol 1,2-dioxygenase, 9027-16-1.

Supplementary Material Available: Table of thermal parameters for $(dabcoH)_2$[Fe(NTA)DBC]·DMF (3 pages). Ordering information is given on any current masthead page.

(45) Lauffer, R. B.; Que, L., Jr. *J. Am. Chem. Soc.* **1982**, *104*, 7324–7325.